Title
ATOMIC RESOLUTION IMAGING IN Al-Li-Cu ALLOY

Authors
Radmilovic, V.
Thomas, G.

Publication Date
1987-06-01

Center for Advanced Materials

CAM

Presented at the 4th International
Aluminum Lithium Conference,
Paris, France, June 10–12, 1987

Atomic Resolution Imaging in Al-Li-Cu Alloy

V. Radmilovic and G. Thomas

June 1987

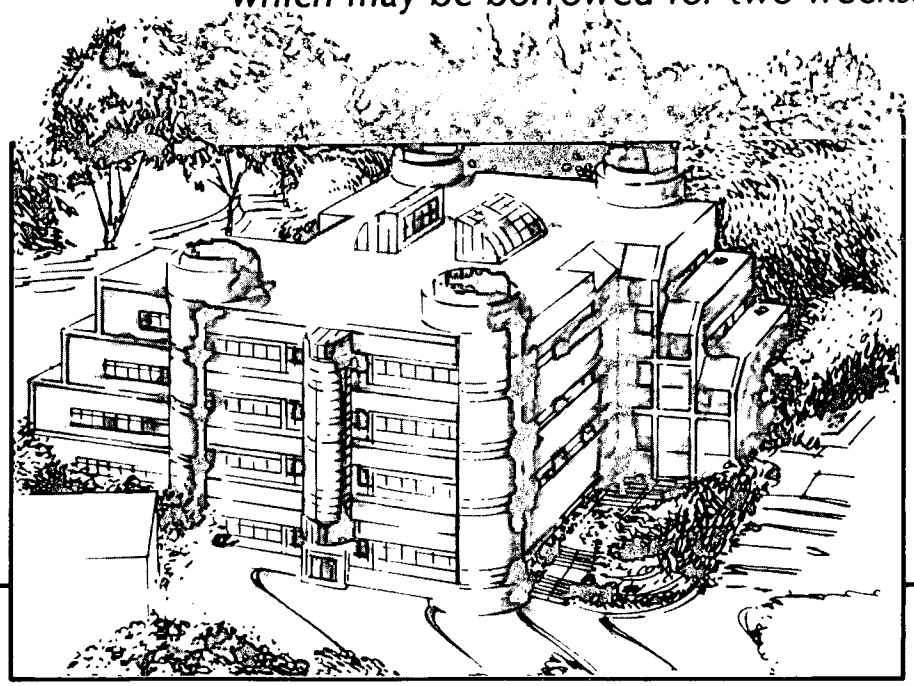

Materials and Chemical Sciences Division

Lawrence Berkeley Laboratory • University of California

ONE CYCLOTRON ROAD, BERKELEY, CA 94720 • (415) 486-4755

Prepared for the U.S. Department of Energy under Contract DE-AC03-76SF00098

DISCLAIMER

ATOMIC RESOLUTION IMAGING IN Al-Li-Cu ALLOY

V. Radmilovic* and G. Thomas
Center for Advanced Materials
Lawrence Berkeley Laboratory
and
Department of Materials Science and Mineral Engineering
University of California, Berkeley, CA, 94720

*Permanent address: University of Belgrade, Department of Physical Metallurgy, Karnegijeva 4, P.P. 494, Belgrade, Yugoslavia,11001.

ABSTRACT

The structure of β'/δ' and T1 precipitates in Al-Li-Cu alloy has been investigated using the atomic resolution electron microscope and computer simulation. Thermal-mechanical processing was done in a program designed to define precipitate nucleation and growth conditions. The results show the β'/δ' complexes are misoriented (1°) $L1_2$ ordered particles. The δ' shell develops polygonal facets around β' core. The T1 phase density is considerably increased by mechanical processing between aging treatments and the results are consistent with increased heterogeneous nucleation, especially by slip within δ' particles. The structure of T1 is proposed to be hexagonal with different composition layers ABCDA, but which are faulted during growth.

1. INTRODUCTION

In the past ten years much useful information on precipitation reaction in Al-Li-Cu alloys has been obtained/1-3/. However, very important details such as the nucleation and growth of coherent and semicoherent precipitates, substructure and morphology of complex precipitates, transformation interfaces, etc., have remained unclear, until recently when new electron microscopy facilities with improved high-resolution and probe- forming capabilities have been available.

Since Hardy and Silcock/4/ first identified the main precipitate phases in the Al-Li-Cu system, characterization of the phases that are responsible for strengthening, such as δ'(Al_3Li) and T1(Al_2CuLi), has received the attention of several research groups/5-9/, but their results have often been controversial. Small additions of Zr to Al-Li base alloys serves to form a metastable cubic Al_3Zr precipitate which retards recrystallisation and controls grain growth. Additionally Zr improves toughness and corrosion resistance/10,11/.It has been claimed that δ'(Al_3Li) precipitates on the β'(Al_3Zr)/matrix interface form "spherical" shell around β'/12-14/. In electron microscopy imaging by dark field using the δ' reflection the β' is not illuminated/12,15/. Gayle and Vander Sande/15/ suggested that this could be due to disordering of an β' core or that Li is incorporated into the Zr sublattice of β', which leads to an intensity reduction through the structure factor. This is in disagreement with the results presented by Stimson et al. /12/. They found, in electron microscopy studies evidence that the "dark imaging" centers are merely β' particles of slightly different (<1°) orientation to the δ' shell. The first part of this paper is concerned with the morphology and atomic substructure of these complex δ'/β' precipitates.

Another important strengthening precipitate, the T1 phase was first analysed by Noble and Thompson/5/ and later in more detail by Huang and

Ardell/9/. In a very detailed diffraction and crystallographic study, they defined T1 in terms of a hexagonal unit cell, as originally suggested by Noble and Thompson/5/, assuming perfect stoichiometry. In this paper the results of a high resolution transmission electron microscopy studies of nucleation and growth T1 semicoherent phase are also presented, in which atomic resolution imaging and computer simulation have been combined to better define the basis of the T1 structure.

2. EXPERIMENTAL PROCEDURE

2.1. Material and Thermo-Mechanical Treatment

The alloy Al-2.35Li-2.49Cu-0.13Zr, provided by ALCOA, has been heat treated as follows: a) solution annealing for 2h at 550°C and ice-brine quenching, b) pre-aged at 175 and 225°C for 1h, c) deformation 10% cold rolling, and d) re-aged at 175 and 225°C for 15h, to produce underaged and overaged alloys. Mechanical properties were measured after each processing route and unusual tensile to yield ratios have been found(2 to 3.5) indicating excellent cold formability. However this paper will discuss only the metallographic aspects of the treatment.

2.2. Specimen Preparation

Discs of 3 and 2.3mm were punched from the slices cut by a slow-speed diamond saw. The specimens were electropolished at the temperature range between -25 and -35°C, in 30% nitric - 70% methanol electrolyte. The voltage was in the range from 9 to 12V, and current from 10 to 20mA. The thin foils were rinsed in redistilled water and pure ethanol, dried and stored under vacuum and were examined on the same day in the electron microscope.

2.3. High-Resolution Transmission Electron Microscopy

Conventional transmission electron microscopy (TEM) has been done on a Philips 400 electron microscope oprerating at 120kV. High resolution transmission electron microscopy (HREM) images were taken on a the JEOL ARM electron microscope operating at 800 and 400kV. Specimen for HREM were tilted into exact zone axis <110> for the analyses of T1 and <001> for analyses of δ'/β' precipitates, using a high precision goniometer. An objective aperture of radius 0.06nm was used to filter out high-order spatial frequencies and to improve image contrast. Through-focus series of images were taken automatically in 8nm increments, starting at the minimum contrast condition. The Sherzer focus value is -60nm with respect to the Gaussian image plane, and is the same at 400kV and 800kV for used Atomic Resolution Microscope.

2.4. Image Simulation

In order to interpret atomic resolution images it is essential to carry out computations for image simulation. Simulated high resolution TEM images of T1 precipitate were calculated using the SHRLI multislice program described by O'Keefe/16/, with microscope parameters: defocus step Δf=8nm, spherical aberation C_s=2.8mm, half-angle value α=0.6mrad, and spread of the focus Δ=8nm, using models based on published data/10/, but modified to correspond to the observed structures and intensities. Simulated HREM images of the composite δ'/β' precipitate were calculated using CEMPAS multislice program described by Kilaas/17/, with microscope parameters the same as in the SHRLI program except that spread of focus was Δ=10nm. Both calculation were done for foil

thickness ranges between 5 and 20nm, and for defocus ranges between -28 and -92nm, with respect to the Gaussian image plane.

2.5. Optical Diffraction

In order to obtain diffraction information from extremely small volumes of investigated samples the laser optical diffraction procedure, developed for the study of aged alloys by Gronsky, Sinclair, and Thomas/18/, has been used.

3. RESULTS AND DISCUSSION

3.1. β'/δ' complex precipitate

Figure 1 shows a typical ARM image of the β'/δ' complex. In agreement with previous results/12-15/ these images confirm that δ' forms a complete shell around the β' precipitate. However, Fig.1 shows also that the δ' shell is not spherical as has been previously reported/19/. Atomic resolution imaging revealed that the δ' shell is truncated with facets leading to polygonal shapes. Fig.1 also shows that on aging δ' particles do not increase in width symmetrically around β' particles as reported previously if β' particles are not in the vicinity of grain or subgrain boundaries/13/.

Direct and accurate measurements on enlarged micrographs show that the superlattice fringes corresponding to {100} reflections of β' and δ' are slightly misoriented, with respect to each other. The misorientation is of the order of 1^{o}. This result thus confirms why β' does not reverse contrast in the δ' dark field images using superlattice reflection. On the other hand it is obviouslly clear from the images that, "dark imaging" centers could not be due to disordering of β' region, which would yield a weak or zero superlattice (100) intensity. Sinclair and Thomas/20/ showed that if the degree of order is less than about 0.5 the superlattice fringes are too weak to be resolved. In Fig. 1, the spherical β' particle also have well defined superlattice structures, so β' remains highly ordered. This result shows the immediate value of direct atomic resolution imaging. An increase in precipitate size with time seems to be due to both growth and coarsening rather than only coarsening as suggested by Makin and Ralf/13/.

Although growth and coarsening reactions differ kinetically, it can be seen in Fig.1 that their influences on the microstructure of coherent phase mixtures is mostly the same, and these two reactions are usually treated without distinction /21/. Warlimont/21/ also suggested that in the absence of significant misfit, coherent particles will grow as determined by their overlapping diffusion fields, but without any further interaction. If the particles are disordered they will coalesce when they impinge. When they are ordered and impinge, they will coalesce only if their sublattices are occupied in phase. Impinging particles whose lattices are antiphase will not merge because the ensuing formation of a common APB would require a higher energy than if a layer of disordered phase was left between them. The reason for that is the same as in the case of heterogeneous nucleation of a disordered phase at an APB, and it is satisfied when the energy condition is $2\mathrm{CPB}\gamma < \mathrm{APB}\gamma$/21/, where γ is the interfacial energy.

Computer simulation (Fig.2) on the bases of perfect ordered crystals of Al_3Li (δ') around Al_3Zr(β') also shows that a dark transition region is present, as a result of destructive interference, even if there is no

misorientation. This prediction is in very good agreement with the experimental results (Fig.1). The atom positions in the simulated image are defined as white spots. The reason for this is that the value of the contrast transfer function(CTF) amplitude for the objective lens defocus value of -90nm, is positive with respect to the Scherzer focus of -60nm. Atom positions give rise to dark contrast when the scattering vector value in both cases is around $5nm^{-1}$, due to phase reversal.

3.2. Heterogeneous nucleation and growth of T1 phase

The main differences between the thermal-mechanically treated and nondeformed aged material is the much increased density of T1 precipitates, and the complete dissolution of the δ' phase in the intense planar slip bands. The increase in the number of T1 nucleation sites in underaged alloy(175^{o}C.1h/10%/15h) (Fig.3) is almost certainly due to heteregeneous nucleation associated with dislocation cutting of δ' particles during the 10% cold rolling. Similar observation in Al-Li-Cu alloys have been reported by Rioja et al/22/. Evidence for this is obtained in the dark field image of a δ' superlattice reflection which also includes one variant of T1 as shown in Fig.4. This figure shows evidence of T1 formed at fresh interfaces on sheared particles. Other authors/14/ also found that δ' precipitates can be cut by T1 and no coarsening of the δ' occurs in the vicinity of T1 particles. Tosten et al./14/ also reported that in the region containing a large number density of T1 precipitates a low number density of the small spherical δ' was present. However, our results show(Fig. 3,5) that it could be a characteristic of Al-Li-Cu alloys only in overaging condition, when T1 precipitates becoming the dominant matrix phase at the expense of θ' (Al_2Cu) and δ', as it has been reported previously(eg., ref. 14,19). Figs. 5, 6 clearly show only small volumes of δ' remaining next to the thickening T1 phase.

T1 is present in two variants $(1\bar{1}1)$ and $(11\bar{1})$ (Fig. 6) with respect to the FCC matrix. This result is the same in the underaged(175^{o}C/1h/10%/15h) and overaged alloy(225^{o}C/1h/10%/15h). It is clear that T1 nucleation sites appear preferentially in underaged alloys inside the ordered δ' phase (Fig. 3). This must caused by plastic flow due to glide on {111}. Only those particles in the matrix {111} glide planes will be affected. Thus dislocation solute atom, or particle interaction for nucleation of T1 is emphasized. These data provide direct evidence for a model proposed by Noble and Thompson/5/ to describe growth of T1 from split unit dislocation. Fig. 7 shows that the δ' phase becomes partially disordered when a unit dislocation passes through. This is in excellent agreement with the theoretical prediction of Khachaturyan and Morris (University of California, Berkeley) for the interaction between glide dislocations and the ordered δ' phase in Al-Li alloys. It is clear therefore that T1 is primarily heterogeneously nucleated as a resut of an appropriate site created by dislocations. The unit translation vector in the FCC superlattice of the type Al_3Li ($L1_2$), (which is the typical slip vector for the close-packed octahedral slip planes) is exactly twice that in the Al-matrix and the superlattice dislocations in δ' thus consist of pairs of a/2<110> without or coupled together by an antiphase boundary (APB), Fig. 8. Each unit dislocation is itself dissociated into a pair of Shockley partials coupled by a complex fault/23/. The equilibrium width of such a superlattice dislocation is determined primarily by a balance between the surface tension of the APB and the mutual repulsion experienced by the pair of a/2<110> dislocation as at a stacking fault/24/.

The structure and morphology of T1 is consistent with the well studied γ' precipitate/25-28/observed in Al-Ag alloys. In order for hcp plates to form from a free matrix a nucleating fault must be created. In Al the

stacking fault energy is high, but the creation of a fault within δ' is the favored provides the necessary nucleating condition, that is analogous to Al-Ag alloys where the hcp γ' phase is only heterogeneously nucleated by dissociation of dislocation effected by diffusion of silver atoms/25, 26/.

Since the present observations have been made in a high voltage microscope it is possible that the defects seen (e.g. Fig. 3) could be radiation damaged induced. They are observed both at 400 and 800kV. In Al the threshold knock-on energy is about 170kV but the value is not known for δ'. Experiments are continuing to establish whether or not displacement damage is a factor in these observations. However the fact that not all δ' particle shows faults or presence of a T1 nucleus suggests that the slip model for T1 nucleation within δ' is probably correct.

Some authors have suggested that the precipitation of T1 hexagonal phase with lattice parameters a=0.496nm and c=0.935nm is preceded by another metastable precipitate called T'/7/, which could be orthorhombic with lattice parameters a=0.287nm, b=0.86nm, and c=0.406nm/6/, or hexagonal with a=0.495nm and c=0.701nm/8/. Laser optical microdiffraction experiments (e.g. Fig. 9) have shown that none of those metastable precipitates is present and this is in agreement with the work of Huang and Ardell /9/.

Computer simulation of T1 has been carried out starting with model of Huang and Ardell but modified to account for the observed fringe intensity. Figure 5 is particularly suggesting a planar sequence ABCDA.. in which the composition of planes B and D are not the same as they are presumed to be in the Al_2CuLi structure of ref.10 in which the layers go ABCBA...The differences are illustrated schematically in Fig. 11. The simulated image of Fig. 12 is seen to be in good agreement with this observations. The composition of plane D corresponds to that for a lower structure factor than that of plane B. Thus the composition of the basic unit cell must be as in Fig. 11.

However the development by growth of T1 does not preserve this ideal sequence. The ledges corresponding to growth every 2nd layer (every other {111} plane must be faulted to create a perfect ABAB... hcp T1 phase) but there are mistakes in this as faulting can be clearly seen (Fig. 10).It is likely that these growth mistakes can account for differing reports on T1, T1' etc., but the basic precipitate is still T1 hcp.

4. SUMMARY

The results of atomic resolution imaging have clarified that β'/δ' complexes are polygonal shaped highly ordered Al_3Li shell around Al_3Zr core slightly misoriented with respect to each other.

T1 is shown to nucleate at stacking faults predominantly in δ' after deformation and grows to be a faulted hexagonal structure of average composition Al_2CuLi.

5. ACKNOWLEDGMENTS

The authors thank Mr. C. Nelson who assisted with the experimental work, Dr. R. Kilaas and Dr. M. O'Keefe for help in computer simulation, and Mr. J. Turner for printing of HREM pictures. This paper is part of a larger program in the Center for Advance Materials dedicated to research on Al-Li based alloys. This work supported by the Director, Office of Energy Research,

Office of Basic Energy Sciences, Materials Sciences Division of the U.S. Department of Energy under contract No. DE-AC03-76SF00098.

6. REFERENCES

1. T. H. Sanders Jr. and E. A. Starke Jr., (eds), "Aluminum-Lithium Alloys" (TMS-AIME, Warrendale, PA, 1981).
2. T. H. Sanders Jr. and E. A. Starke Jr., (eds), "Aluminum-Lithium Alloys II" (TMS-AIME, Warrendale, PA, 1984).
3. C. Baker, P. J. Gregson, S. J. Harris, and C. J. Peel, (eds), "Aluminum-Lithium Alloys III" (The Institute of Metals, London, 1986).
4. H. K. Hardy and J. M. Silcock, J. Inst. Met., 1955-56, **84,** 423.
5. B. Noble and G. E. Thompson, Met. Sci. J.,1972, **6**, 167.
6. R. J. Rioja and E. A. Ludwiszak, p.471 in ref. 3.
7. H. Suzuki, M. Kanno, and N. Nayashi, J. Jpn. Inst. Light Met., 1982, **32**, 88.
8. A. K. Eikum and G. H. Narayanan, Proceed. of the 44th EMSA Annual Meeting, G.W. Bailey, Ed.,San Francisco Press, 1986, p. 550.
9. J. C. Huang and A. J. Ardell, Mat. Sci. and Tech., 1987, **3**, 176.
10. E. Ness and N. Ryum, Scripta Metall., 1971, **5,** 987.
11. E. Ness, Acta Metall., 1972, **20**, 499.
12. W. Stimson, M. H. Tosten, P. R. Howell, and D. B. Williams, p.386 in ref 3.
13. P. L. Makin and B. Ralph, J. Mat. Sci., 1984, **19**, 3835.
14. M. H. Tosten, A. K. Vasudevan, and P. R. Howwell, p. 483 in ref. 3.
15. F. W. Gayle and J. B. Vander Sande, Scripta Metall., 1984, **18**, 473.
16. M. A. O'Keefe, Electron Optical Systems, SEM Inc., AMF O'Hare, Chicago, IL,1985, p. 209.
17. R. Kilaas, Proceed. of MAS 1987, in press.
18. R. Gronsky, R. Sinclair, and G. Thomas, Acta Met.,1976, **24**, 789.
19. J. M. Galbraith, M. H. Tosten, and P. R. Howell, J. Mat. Sci., 1987, **22**, 27.
20. R. Sinclair and G. Thomas, Proceed. of 32nd EMSA, 1974, p.500.
21. H. Warlimont, "Electron Microscopy and Structure of Materials", G. Thomas, ed., University of California Press, 1972, p.505.
22. R. J. Rioja, P. E. Bretz, R. R. Sawtell, W. H. Hunt, and E. A. Ludwiczak, Proceed. Conf. on Al-alloys, University of Virginia, 1986, vol.III,p.1781
23. M. J. Marcinkowski, N. Brown, and R. M. Fisher, Acta Metall.,1961,**9**, 129.
24. J. M. Oblak and B. H. Kear, "Electron Microscopy and Structure of Materials", G. Thomas, ed., University of California Press, 1972, p.566.
25. J. A. Hren and G. Thomas, Met. Trans., 1963, **227**, 308.
26. G. R. Frank, D. Robinson, and G. Thomas, J. Appl. Phys., 1961, **32**, 1763.
27. J. M. Howe, U. Dahmen, and R. Gronsky, Phil. Mag.,A., in press.
28. J. M. Howe, Proceed. of EMSA 1987, in press.

7. FIGURE CAPTIONS

Fig. 1. Atomic resolution image of δ'/β' particles; polygonal morphology of the δ' shell; overaged condition; zone axis [100].

Fig. 2. Simulated high-resolution TEM image of a δ'/β' complex particle in Al matrix (a); white spots represent atom positions. Projected potential for same particle (b); black spots represent atom positions.

Fig. 3. Atomic resolution image of deformed (arrow D) and non deformed (arrow N) δ' particles in the underaged condition; zone axis [110].

Fig. 4. CDF image of a δ' superlattice reflection which also includes one variant of T1 phase.

Fig. 5. Atomic resolution image of a δ' in a vicinity of a T1 phase; overaged alloy; zone axis [110].

Fig. 6. Atomic resolution image of the two variants T1 phase (111) and (11̄1); overaged alloy; zone axis [110].

Fig. 7. Atomic resolution image of a partially disordered δ' after passing a dislocation; underaged alloy; zone axis [110].

Fig. 8. Atomic resolution image of an APB formation after passing a dislocation through δ' superlattice; underaged alloy; zone axis [110].

Fig. 9. Laser optical microdiffraction of a HREM image of a perfect T1 phase.

Fig. 10. Atomic resolution image of a faulted T1 phase; zone axis [110].

Fig. 11. Schematic illustration of a difference between UCB and UCLA/ref. 9/ models of the T1 phase with stacking sequences ABCDA and ABCBA, respectivelly.

Fig. 12. Simulated high resolution image of a T1 phase with stacking sequence: ABCDA (a); Projected potential for same particle (b); The inset shows the atomic resolution image of a perfect T1 phase.

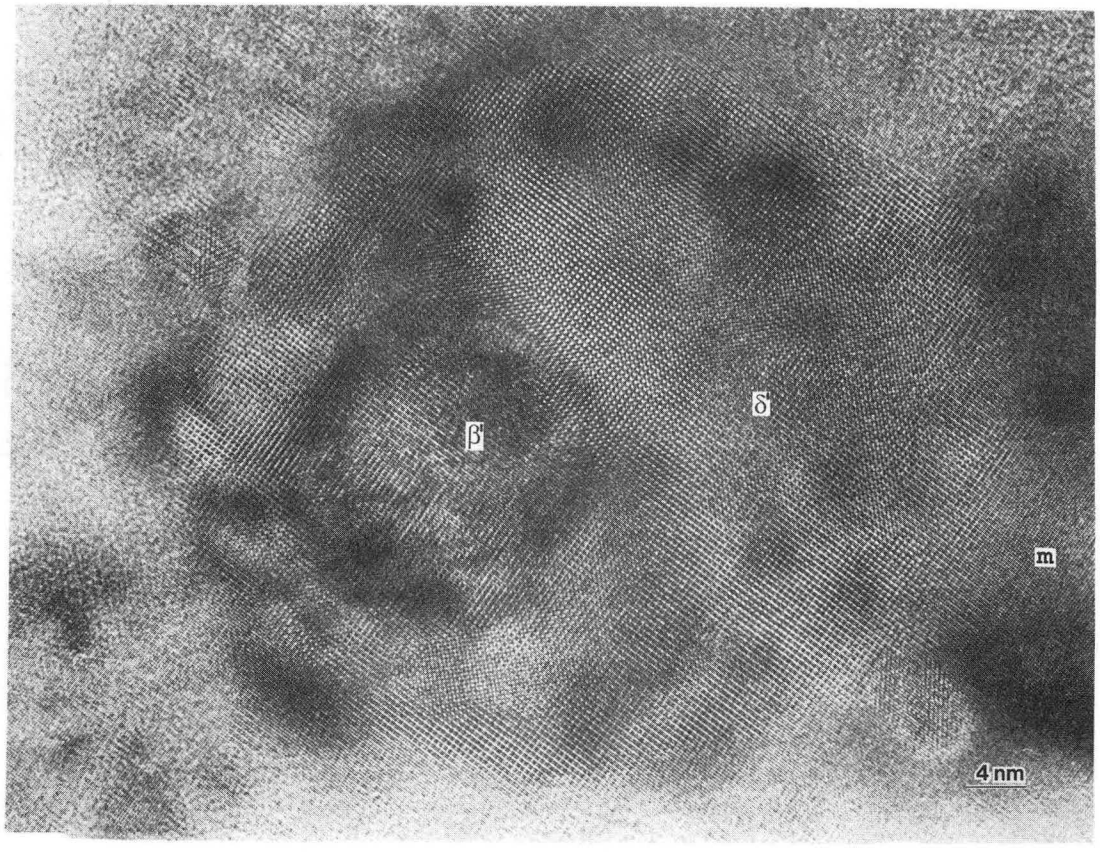

Fig. 1

XBB 875-3898

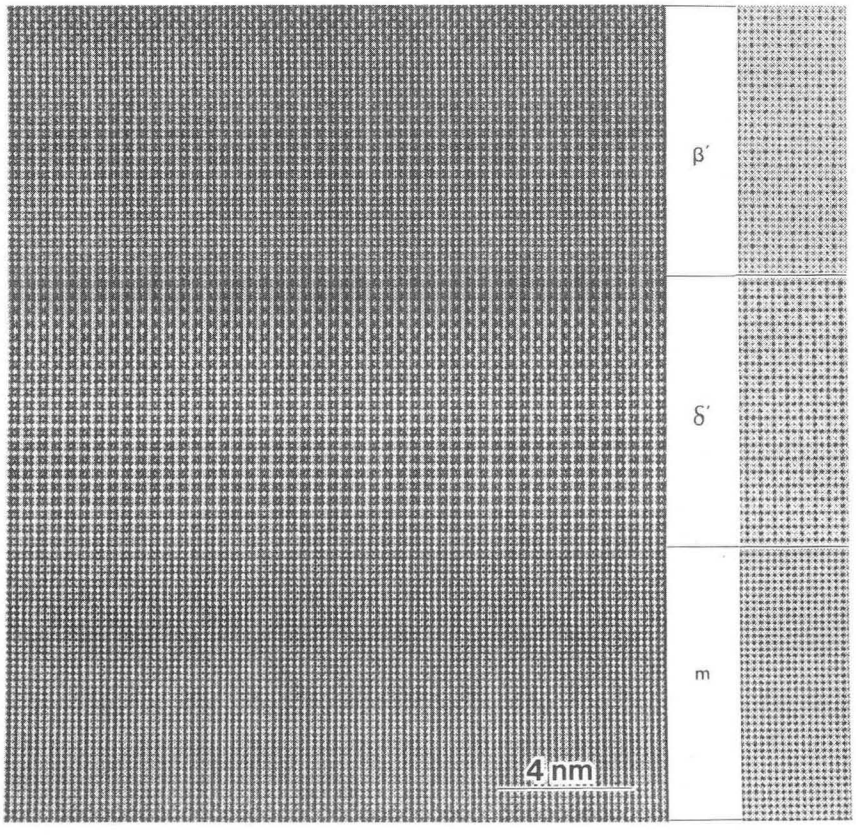

Fig. 2

XBB 875-3897

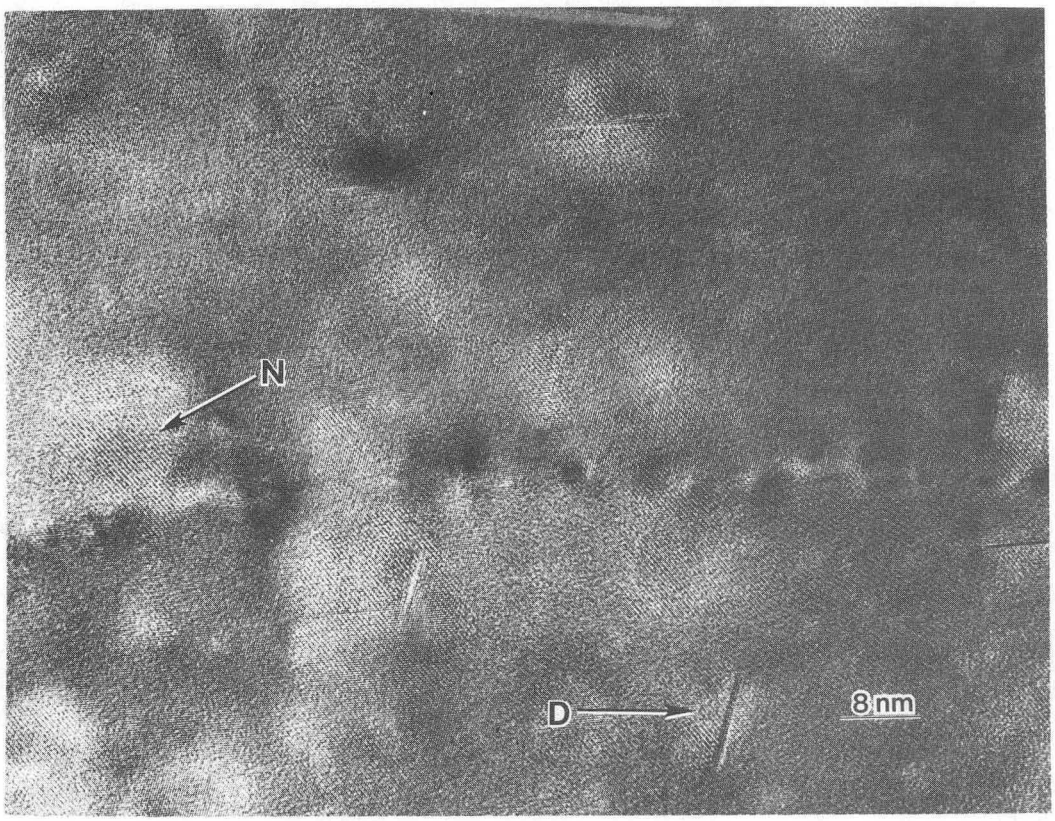

Fig. 3

XBB 875-7053

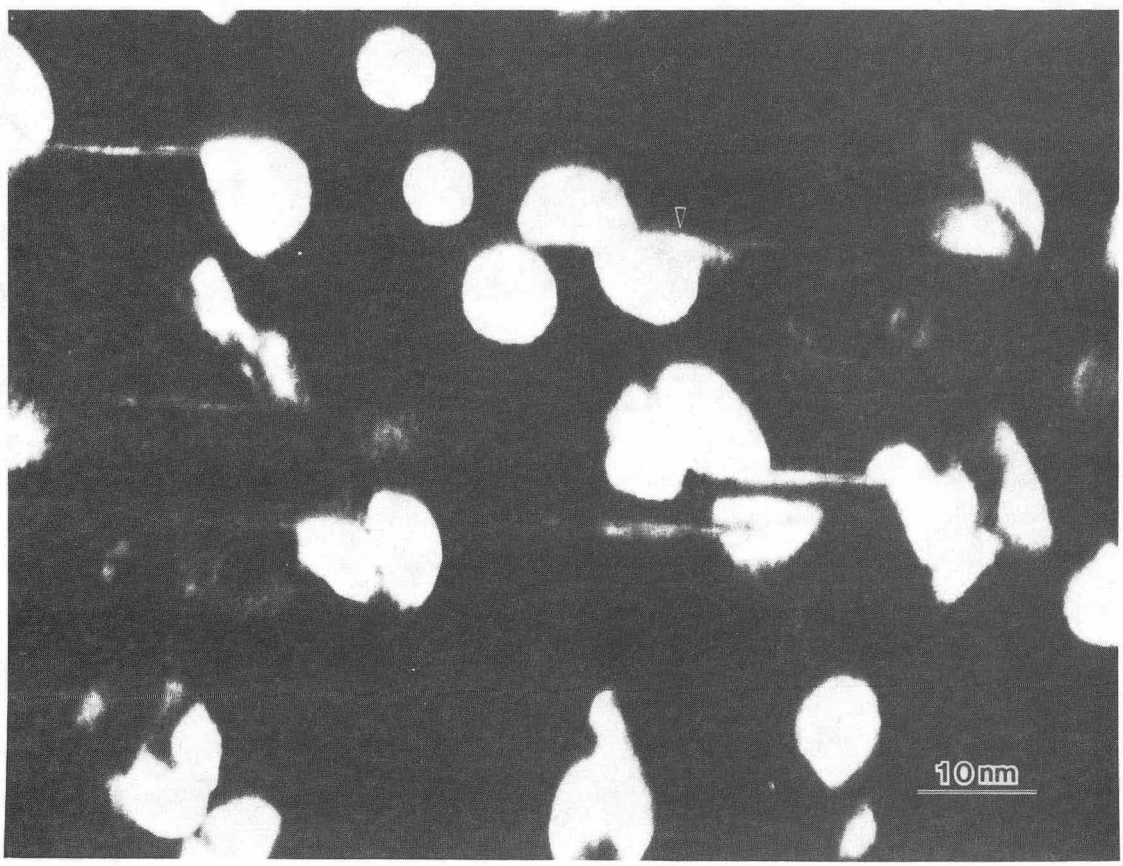

Fig. 4

XBB 874-3199

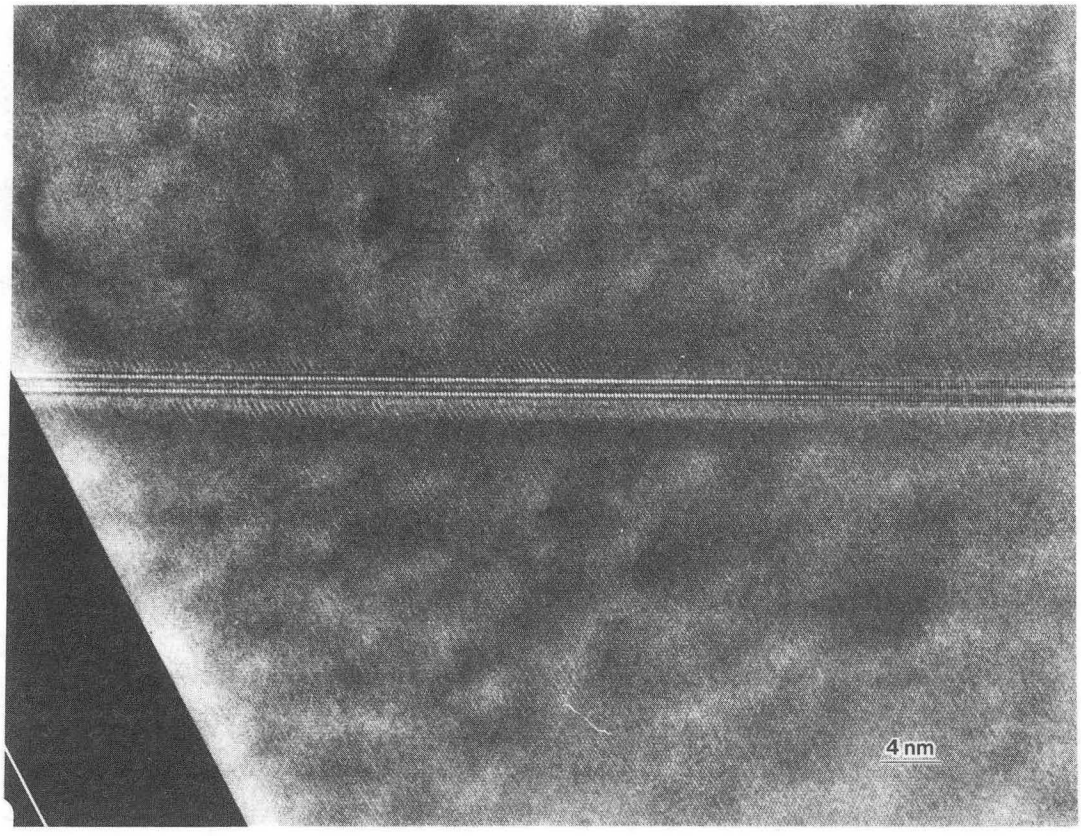

Fig. 5

XBB 874-3174

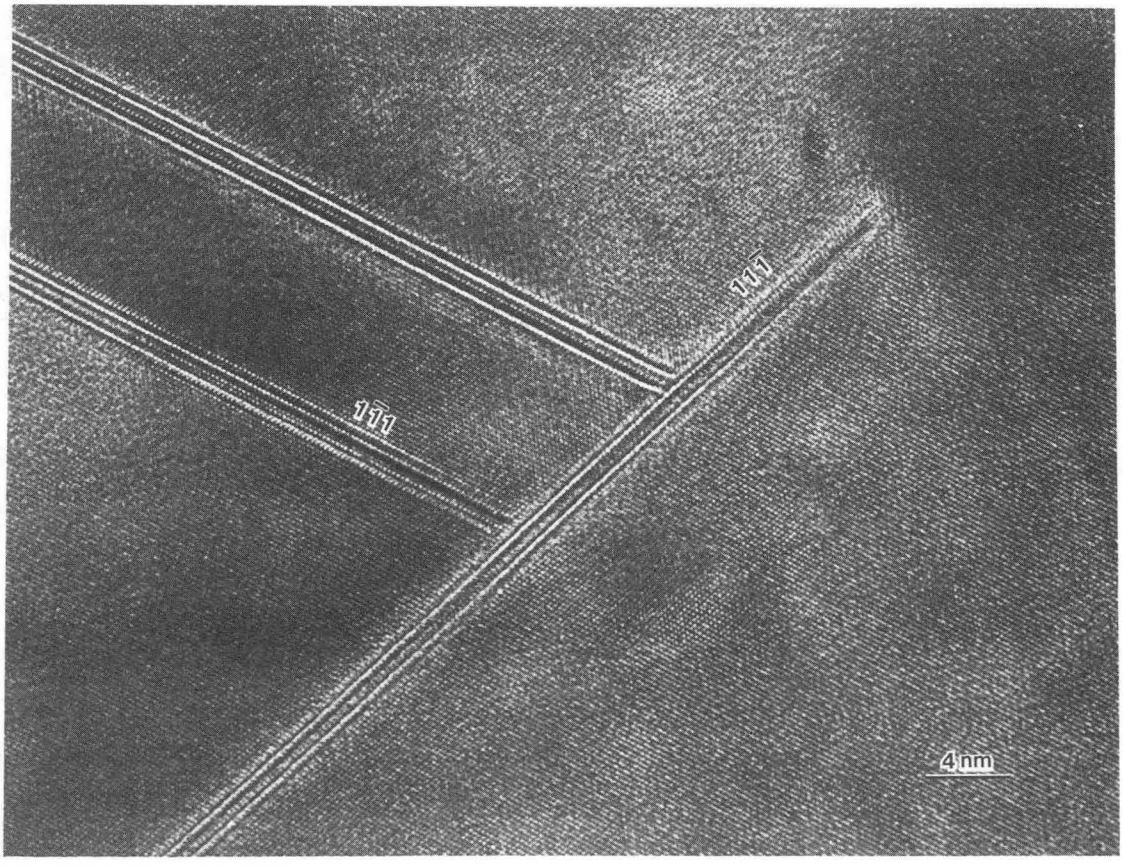

Fig. 6

XBB 874-3191

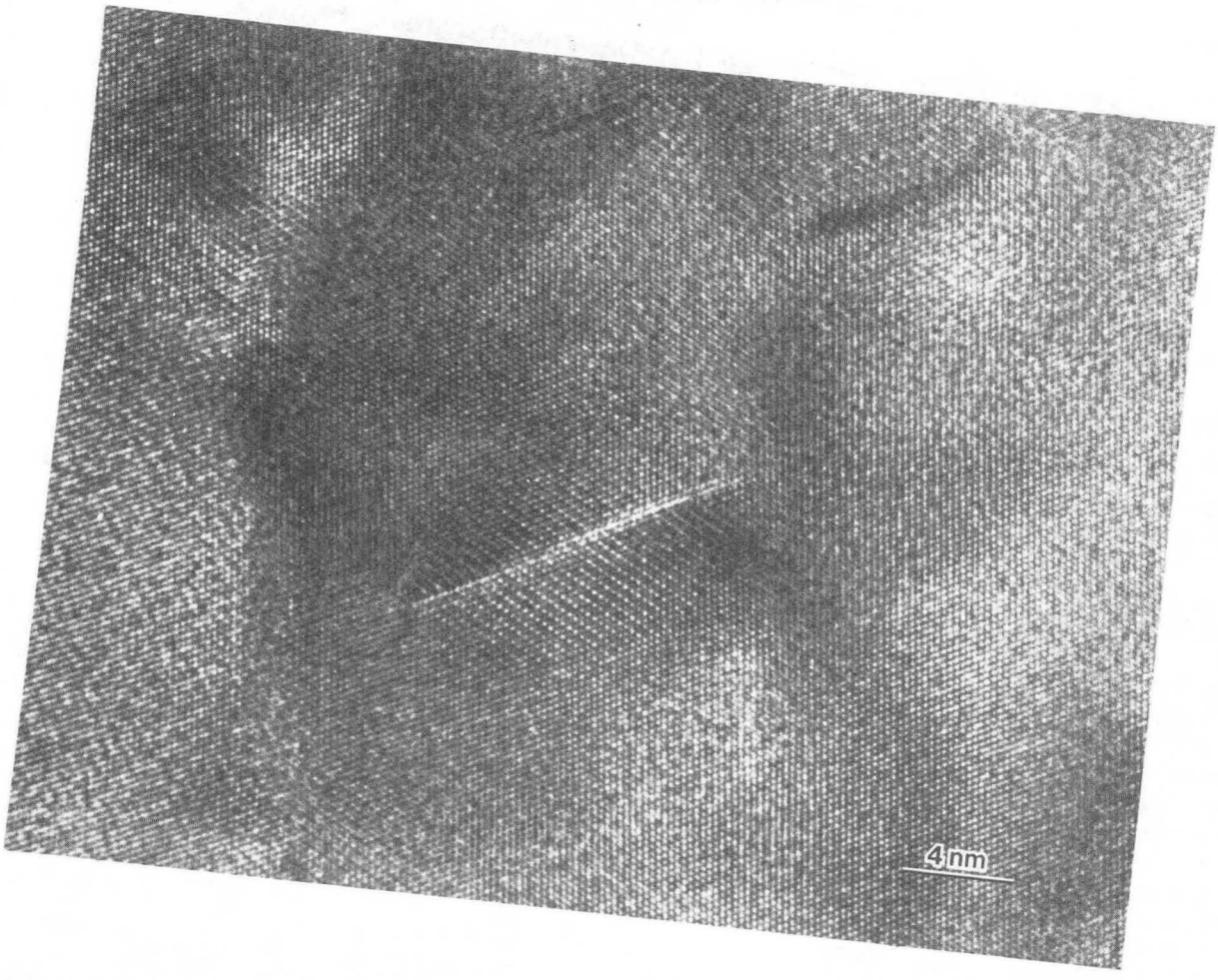

Fig. 7

XBB 874-3172

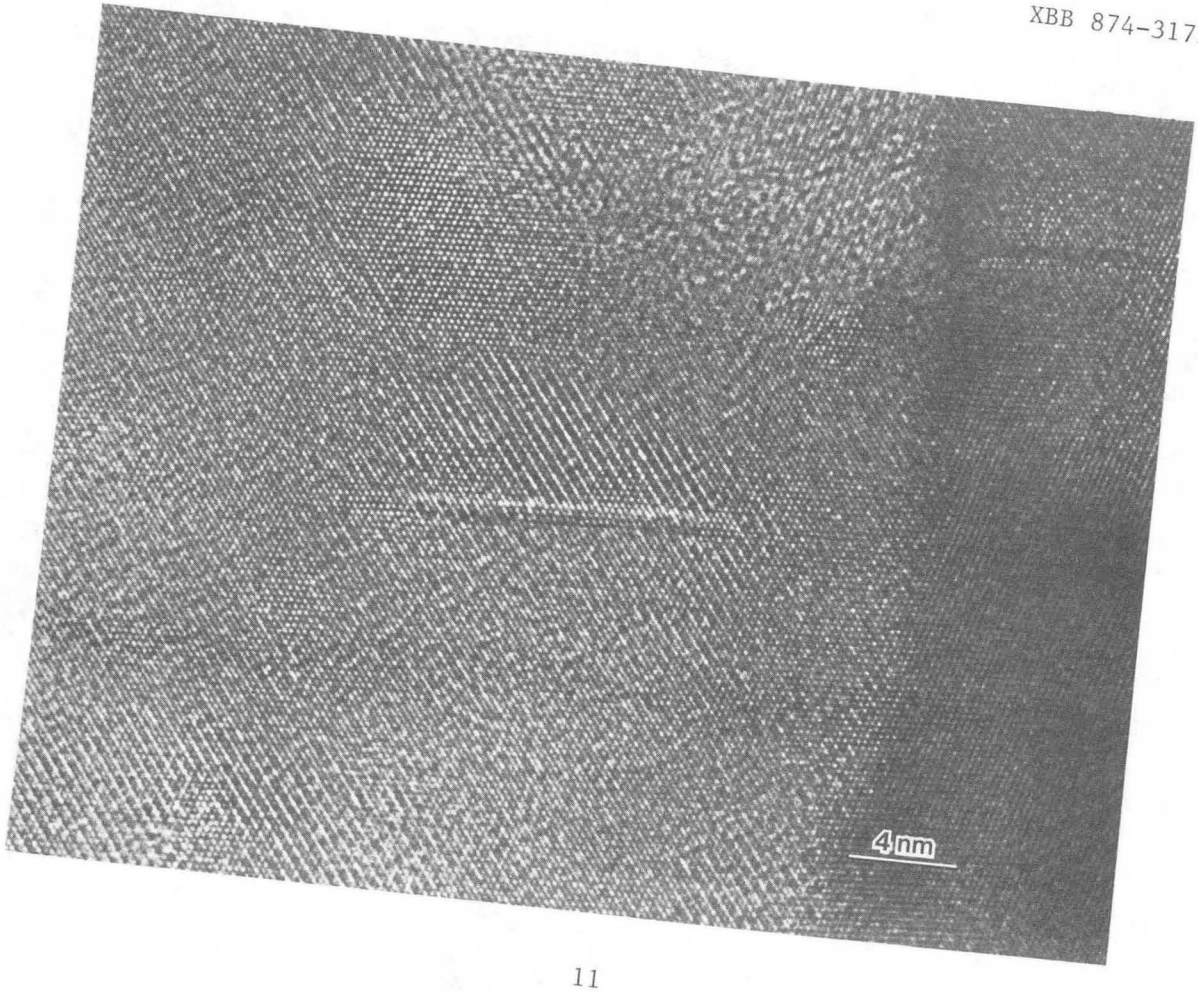

Fig. 8

XBB 874-3187

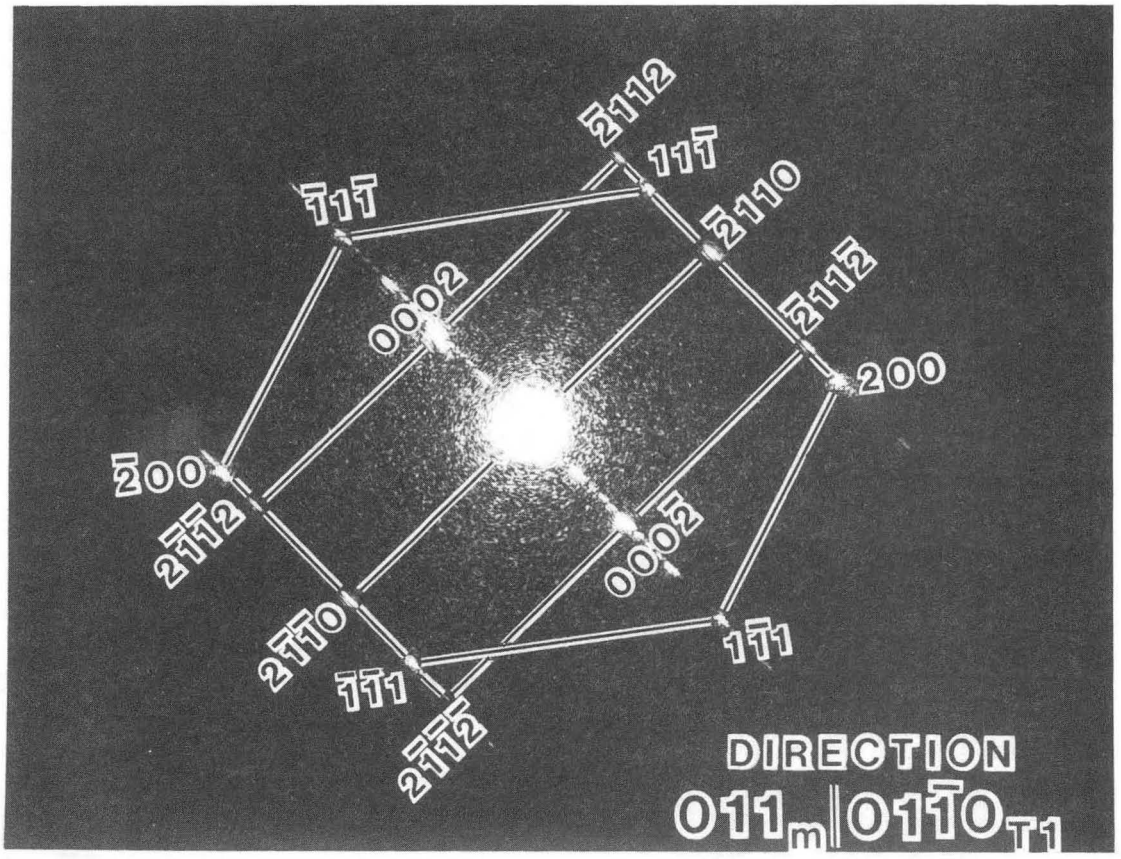

Fig. 9

XBB 875-7071

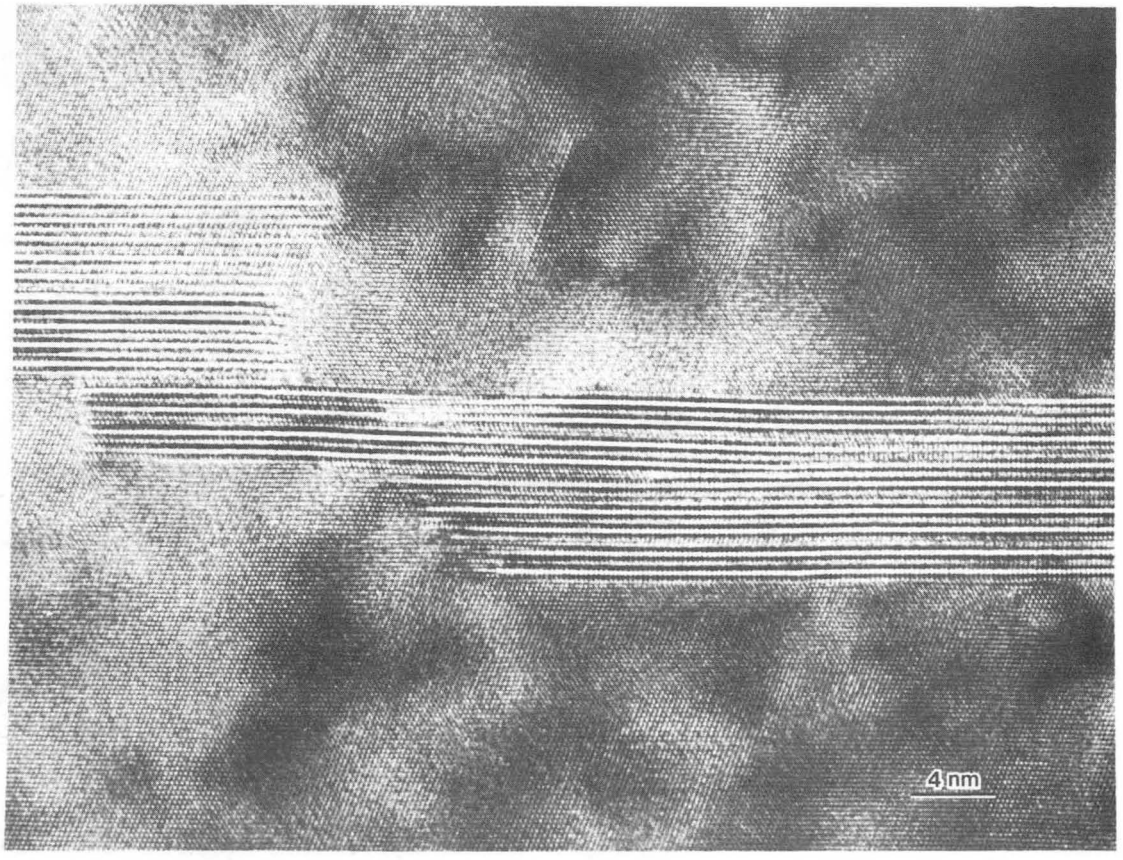

Fig. 10

XBB 874-3175

$T1(Al_2CuLi)$

UCB MODEL				UCLA MODEL			
layer	number of atoms			layer	number of atoms		
	Al	Li	Cu		Al	Li	Cu
A	1.5	3	-	A	1.5	3	-
B	6	-	3	B	4.5	-	4.5
C	6	3	-	C	6	3	-
D	3	-	6	B	4.5	-	4.5
A	1.5	3	-	A	1.5	3	-

Fig. 11

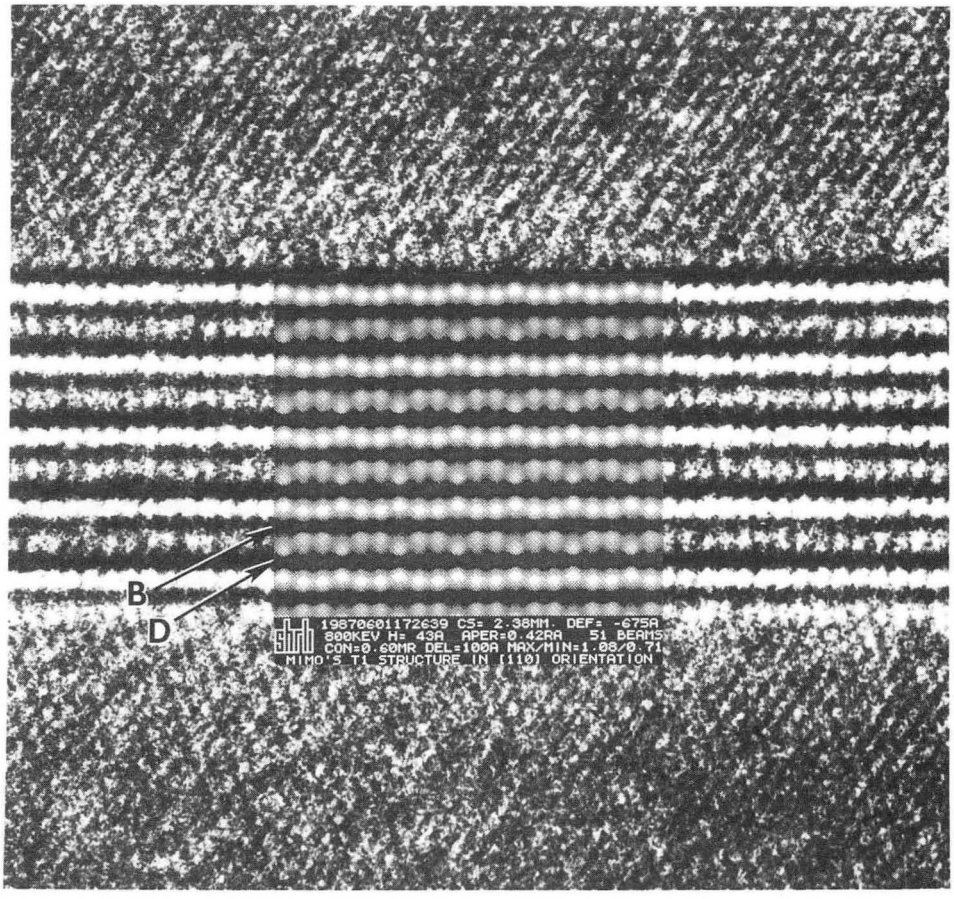

Fig. 12

XBB 874-3176A

LAWRENCE BERKELEY LABORATORY
TECHNICAL INFORMATION DEPARTMENT
UNIVERSITY OF CALIFORNIA
BERKELEY, CALIFORNIA 94720